Onset of multiferroicity in prototypical single spin cycloid BiFeO 3 thin films

Pauline Dufour, Amr Abdelsamie, Johanna Fischer, Aurore Finco, Angela Haykal, Martin Sarott, Sara Varotto, Cécile Carrétéro, Sophie Collin, Florian Godel, et al.

Onset of multiferroicity in prototypical single spin cycloid $BiFeO_3$ thin films

*Pauline Dufour[1]‡, Amr Abdelsamie[1,2]‡, Johanna Fischer[1], Aurore Finco[2], Angela Haykal[2], Martin F. Sarott[3], Sara Varotto[1], Cécile Carrétéro[1], Sophie Collin[1], Florian Godel[1], Nicolas Jaouen[4], Michel Viret[5], Morgan Trassin[3], Karim Bouzehouane[1], Vincent Jacques[2], Jean-Yves Chauleau[5], Stéphane Fusil[1, 6], Vincent Garcia[1]**

[1]Unité Mixte de Physique, CNRS, Thales, Université Paris-Saclay, 91767 Palaiseau, France

[2]Laboratoire Charles Coulomb, Université de Montpellier and CNRS, 34095 Montpellier, France

[3]Department of Materials, ETH Zurich, 8093 Zurich, Switzerland

[4]Synchrotron SOLEIL, 91192 Gif-sur-Yvette, France

[5]SPEC, CEA, CNRS, Université Paris-Saclay, 91191 Gif-sur-Yvette, France

[6]Université d'Evry, Université Paris-Saclay, 91000 Evry, France

Abstract. In the room-temperature magnetoelectric multiferroic, $BiFeO_3$, the non-collinear antiferromagnetic state is coupled to the ferroelectric order, opening applications for low-power electric-field-controlled magnetic devices. While several strategies have been explored to simplify the ferroelectric landscape, here we directly stabilize a single domain ferroelectric and spin cycloid state in epitaxial $BiFeO_3$(111) thin films grown on orthorhombic $DyScO_3$(011).

Comparing with films grown on $SrTiO_3$(111), we identify anisotropic in-plane strain as a powerful handle to tailor the single antiferromagnetic state. In this single domain multiferroic state, we establish the thickness limit of the coexisting electric and magnetic orders and directly visualize the suppression of the spin cycloid induced by the magnetoelectric interaction below the ultrathin limit of 1.4 nanometers. This as-grown single domain multiferroic configuration in $BiFeO_3$ thin films opens an avenue both for fundamental investigations and for electrically-controlled non-collinear antiferromagnetic spintronics.

Keywords: multiferroic, antiferromagnetic, ferroelectric, anisotropic strain, critical thickness, $BiFeO_3$

Information and communication technologies are currently facing tremendous challenges related to the miniaturization of electronic circuitry and associated increase in energy consumption. This triggers beyond complementary metal-oxide semiconductor (CMOS) paradigms to pursue the progress toward energy-efficient and scalable electronic devices. For instance, magnetoelectric spin-orbit (MESO) devices based on electric field writing of a magnetic bit using ferromagnetic/magnetoelectric bilayers, and spin-to-charge electrical readout have been proposed by industrial leaders such as INTEL.[1,2] Over the last two decades, $BiFeO_3$ has been the paramount multiferroic thanks to its key assets such as room-temperature coexisting ferroelectric and antiferromagnetic orderings and strong magnetoelectric coupling.

In bulk, $BiFeO_3$ exhibits rhombohedral distortion (R3c space group), giving rise to four ferroelastic variants corresponding to eight possible ferroelectric domain states, with

polarization lying along <111> (pseudo-cubic notation used by default).[3] It is also a G-type antiferromagnet with an additional antisymmetric magnetoelectric interaction that stabilizes an incommensurate spin cycloid, with propagation vectors along the <-110> directions,[4,5] so that each ferroelectric domain can harbor three different energetically-degenerate antiferromagnetic cycloidal domains.[6]

In thin-film form, while the influence of epitaxial strain on the ferroelectric domain engineering has attracted tremendous attention,[7–9] the investigation of the antiferromagnetic order only recently boomed with the development of ultrasensitive neutron[10–13] or synchrotron[14–17] experiments as well as scanning magnetometry[18–20] techniques. The substrate-induced epitaxial strain can either trigger a non-collinear cycloidal spin texture or a pseudo-collinear canted G-type antiferromagnetic ordering for low and high strain values, respectively.[19,21] Such a polar and magnetic complexity challenges the quest for deterministic magnetoelectric switching in $BiFeO_3$, and hence has been hindering the integration of multiferroics in CMOS competitive technologies.

The currently most promising approach has involved the integration of (001) thin films of $BiFeO_3$ grown on $DyScO_3(110)_o$ ('o' stands for orthorhombic) substrates. Here, the ferroelectric landscape is reduced to a striped ferroelectric domain pattern with only two ferroelastic variants separated by 71° domain walls.[8] In this configuration, the magnetoelectric coupling results in a zig-zag pattern of antiferromagnetic spin cycloids with two in-plane propagation vectors.[18–20] On the one hand, an electric-field controllable net polarization emerges in the films.[22,23] On the other hand, the accompanying antiferromagnetic order remains non trivial due to the different long range periodic cycloids (64 nm) resulting from the ferroelectric domains.[18] Thus, despite

tremendous progress, a deterministic magnetoelectric coupling remains to be demonstrated in such nanoscale MESO devices.[24]

Here we report on the stabilization of epitaxial thin films of $BiFeO_3$(111) with a single spin cycloidal state. Combining a crystalline orientation favoring a single-domain polarization,[7,15] and strain anisotropy in the film plane,[17] breaks the degeneracy of the antiferromagnetic variants and stabilizes a single-domain multiferroic configuration. Furthermore, taking advantage of this model system, we monitor the onset of the concomitant ferroelectric and magnetic orders from a thickness of 6 unit cells (1.4 nm). Our work establishes the fundamental limits of room-temperature multiferroicity and sets the foundations of multiferroic materials with application-relevant controlled order parameter configurations.

The single-domain ferroelectric configuration tends to form when growing $BiFeO_3$ thin films in the (111) orientation.[7,25] Along this line, the experimental studies in (111)-oriented $BiFeO_3$ relaxed films (1-μm-thick) demonstrated single domain ferroelectric with either multidomain[15,16] or single domain spin cycloids.[17] However, according to Waterfield Prize et al., "the presence of a finite population of minority ferroelastic domains presents a potential hurdle in realizing" devices.[17]

We therefore start our investigation by probing the antiferromagnetic configuration in $BiFeO_3$(111) films grown epitaxially on $SrTiO_3$(111). All our films were grown by pulsed laser

deposition using $SrRuO_3$ as a buffer electrode (Methods). X-ray diffraction indicates a (111) orientation for $BiFeO_3$ and Laue fringes attest for the high crystalline quality of the films (Figure S1). Piezoresponse force microscopy (PFM) reveals a single out-of-plane variant with downward polarization while no in-plane signal could be detected (**Figure 1**b, Figure S1b). The $BiFeO_3$ thin films thus present a single ferroelectric state with a vertical polarization pointing downward (as sketched in Figure 1a).

We then used scanning nitrogen-vacancy (NV) magnetometry to image the magnetic stray field produced by the antiferromagnetic textures of the $BiFeO_3$(111) thin films. Despite the single ferroelectric domain state, a complex magnetic landscape appears (**Figure 2**c, left), consisting of periodic magnetic stray fields with propagation directions varying in space, over typical length scales of few hundred nanometers. This periodic magnetic stray field is the signature of the antiferromagnetic spin cycloid of $BiFeO_3$.[6,18–20] Considering the (111) orientation of $BiFeO_3$ with the polarization along the growth axis for both films, we expect all the antiferromagnetic spin cycloids to propagate in the (111) film plane. For the bulk, the three propagation vectors, k_1, k_2, k_3, are degenerate along the high-symmetry crystallographic <-110> directions of the (111) plane.[5] As the $BiFeO_3$ film is grown under an isotropic in-plane compressive strain of -0.67 $\pm$ 0.03% on $SrTiO_3$(111) (Figure 1c-d), the degeneracy between the three k vectors is not lifted (Figure 2a), giving rise to this multi-k magnetic pattern (Figure 2c, left). This complex magnetic lamellar pattern exhibits a resemblance to the magnetic landscape observed at the surface of $BiFeO_3$ single crystals,[6] here with smaller antiferromagnetic domains.

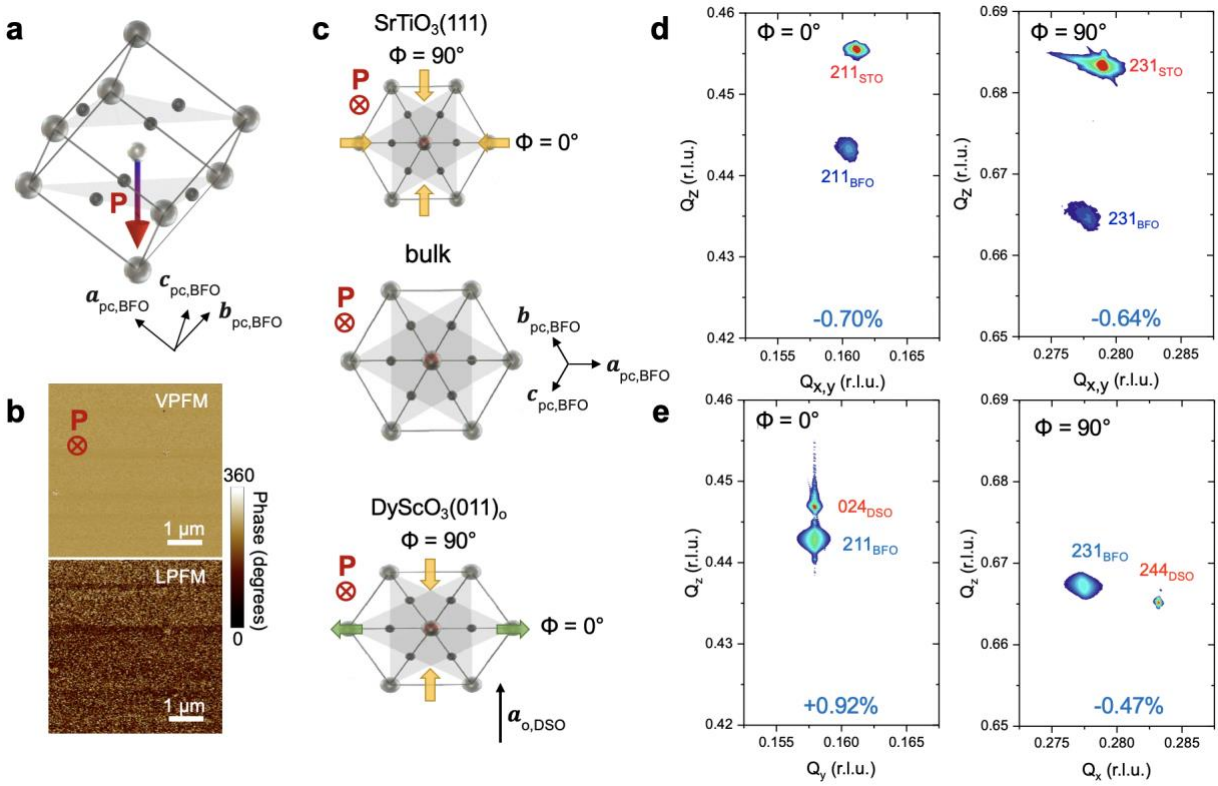

Figure 1. Single domain ferroelectric $BiFeO_3(111)$ thin film under isotropic or anisotropic in-plane strain. a) Sketch of the (111) pseudo-cubic unit-cell with the vertical polarization pointing downward. b) Vertical (V) and lateral (L) PFM phase images indicating a purely vertical polarization as sketched in (a). c) Sketches of the hexagonal lattice of $BiFeO_3(111)$, for the bulk (middle) and films grown on $SrTiO_3(111)$ under isotropic compressive strain (top) or $DyScO_3(011)_o$ under anisotropic in-plane strain (bottom). The yellow and green arrows indicate compressive and tensile strain, respectively. Φ is the in-plane angle relative to the horizontal [100] axis of $BiFeO_3$. d) Reciprocal space maps along the (211) and (231) peaks of $SrTiO_3$, with the corresponding (211) and (231) peaks of $BiFeO_3$. The film is under an isotropic in-plane strain as sketched in c. The corresponding in-plane strain values are displayed at the bottom. e) Reciprocal space maps along the $(024)_o$ and $(244)_o$ peaks of $DyScO_3$, with the corresponding (211) and (231)

peaks of $BiFeO_3$. The film is fully strained at $\Phi = 0°$ and partially relaxed at $\Phi = 90°$, giving rise to a distorted (111) cell as sketched in (c). The corresponding in-plane strain values are displayed at the bottom.

We propose that breaking the isotropic in-plane strain in the (111) plane will lift the degeneracy in the k vector propagation while maintaining a single ferroelectric domain state. We thus move on to the study of $BiFeO_3$ thin films grown on $DyScO_3(011)_o$ substrates, using $SrRuO_3$ as a buffer layer. On these substrates, we highlight that the film quality is strongly dependent on the $SrRuO_3(111)$ surface morphology and the absence of this buffer layer results in a three-dimensional growth for $BiFeO_3$.[26] We found that the optimum surface morphology could be obtained by growing first only two unit cells of $SrRuO_3$ on $DyScO_3$. The initial growth of the $BiFeO_3$ thin film could be monitored using reflection high-energy electron diffraction (RHEED). X-ray diffraction indicates a (111) orientation with high crystalline quality for the $BiFeO_3$ thin films (Figure S2). A reciprocal space map collected around the $(024)_o$ peak of $DyScO_3$ indicates that $BiFeO_3$ is fully strained by the substrate along that direction (Figure 1e). This is not the case when rotating the sample by 90° where the map around the $(244)_o$ peak of $DyScO_3$ shows strain relaxation for $BiFeO_3$. Comparing the in-plane positions of the $BiFeO_3$ peaks with bulk values, we estimate the in-plane strain to be +0.92% and -0.47% perpendicular and parallel to the a_o axis of $DyScO_3$. This anisotropic in-plane strain results in a distortion of the hexagonal (111) unit cell, as sketched in Figure 1c. In addition, PFM reveals the persistence of a single out-of-plane variant with downward polarization and the absence of in-plane signal (Figure S2).

In order to assess the impact of the anisotropic in-plane strain on the spin cycloid propagation, we used scanning NV magnetometry to image the magnetic pattern of $BiFeO_3$ grown on $DyScO_3(011)_o$. Strikingly, the periodic magnetic stray field exhibits a highly ordered texture (Figure 2c, right), which corresponds to a unique vertical propagation vector. Here, the anisotropic in-plane strain of $BiFeO_3$ epitaxially grown on $DyScO_3(011)_o$ lifts the degeneracy between k_2 and k_1, k_3 (Figure 2a, right). This in-plane anisotropy hence gives rise to a single antiferromagnetic spin cycloid propagating along k_2 (Figure 2c, right). The fact that compressive strain along a_o favors the corresponding k_2 variant in $BiFeO_3(111)$ is somehow similar to the preferential in-plane k_1 variant favored for a $BiFeO_3(001)$ film grown under biaxial compressive strain on $DyScO_3(110)_o$.

To obtain an application-relevant, macroscopic picture of the sample magnetic state, we used resonant elastic X-ray scattering (REXS). While scanning NV magnetometry typically scans surface regions of 1 μm^2, the surface area probed using REXS is 10^3-10^4 larger. The dichroic diffraction pattern at the Fe L edge is displayed in Figure 2d for the $BiFeO_3$ thin films grown on $SrTiO_3(111)$ and $DyScO_3(011)_o$. For the films grown on $SrTiO_3(111)$, the dichroic pattern displays a circle around the specular reflection with a diameter corresponding to a periodicity of about 68 ± 2 nm (Figure 2d, left). This suggests that the cycloid propagation is not fully locked to the <-110> high symmetry crystal axes (Note S1, Figure S3), as recently observed at the surface of $BiFeO_3$ single crystals.[6] In contrast, a very clear pair of intense spots at +q and -q, symmetric with respect to the specular beam, is observed on the REXS pattern of $BiFeO_3$ grown on $DyScO_3(011)_o$ (Figure S4),

as expected for a periodic antiferromagnetic structure with a single propagation direction all over the probed area. In addition, the spots show a very strong magnetic circular dichroism (Figure 2d, right), which corroborates the presence of a unique chiral object such as the antiferromagnetic spin cycloid of $BiFeO_3$.[27] Thus, both REXS and scanning NV magnetometry confirm the presence of a single spin cycloid in the $BiFeO_3(111)$ films grown on $DyScO_3(011)_o$. From the diameter of the circle defined by the pair of spots in reciprocal space (Figure 2d), we estimate the spin cycloid period to be 75.7 ± 2 nm. This nicely corroborates the estimated period of 78 ± 5 nm determined in real space using scanning NV magnetometry.

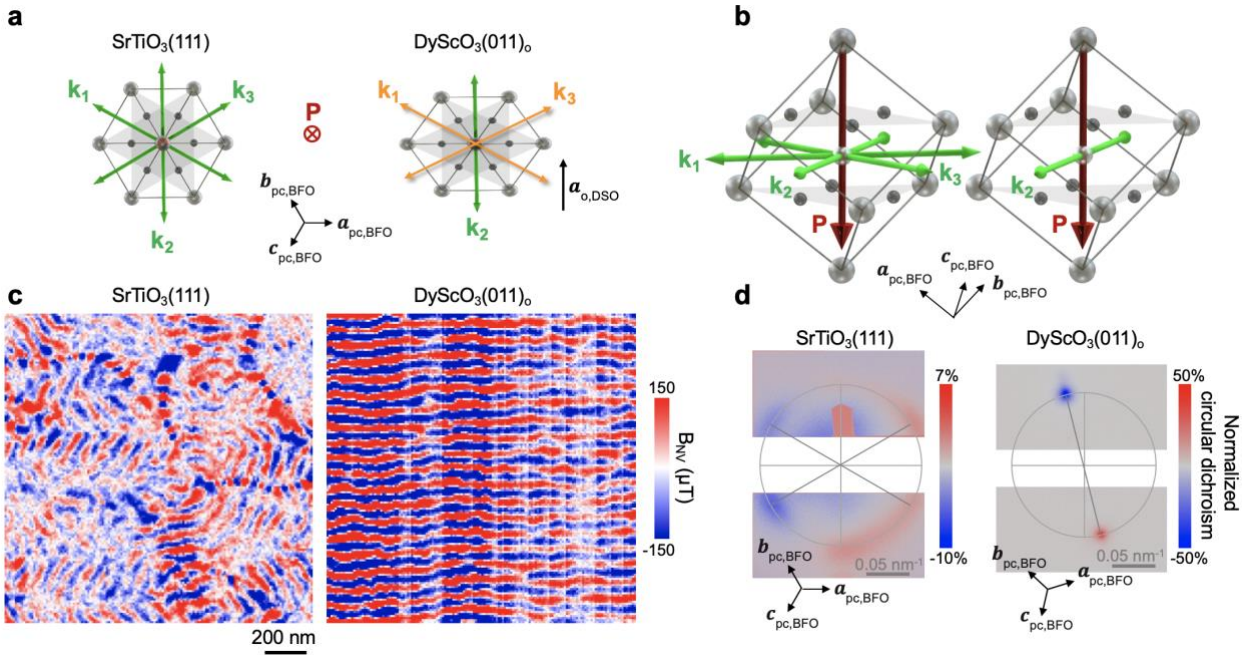

Figure 2. Tailoring a single antiferromagnetic spin cycloid propagating along a_o of $DyScO_3$. a) Sketch of the 3 propagation vectors, k_1, k_2, k_3, for the $BiFeO_3$ film grown under isotropic strain on $SrTiO_3(111)$ and for the film under anisotropic strain on $DyScO_3(011)_o$. While the 3 vectors are degenerate for the first case, the anisotropic in-plane strain lifts the degeneracy between k_2 and

k_1,k_3 for the latter. b) Sketch of the multiple or single antiferromagnetic domain structures with the polarization vertical and the propagation vectors of the cycloid in the film plane. c) Scanning NV magnetometry images of 30-nm-thick $BiFeO_3$(111) on $SrRuO_3$-buffered $SrTiO_3$(111) and $DyScO_3(011)_o$. d) Resonant elastic X-ray scattering dichroic pattern at the Fe L edge for $BiFeO_3$(111) on $SrTiO_3$(111) (left) and $DyScO_3(011)_o$ (right). The film grown on $SrTiO_3$(111) displays a complex dichroic pattern, describing a circle, while the film grown on $DyScO_3(011)_o$ shows a single pair of spots with a strong circular dichroism. This is the signature of a single chiral spin cycloid with propagation vector in the film plane.

By engineering the anisotropic in-plane strain in $BiFeO_3$(111) films, we are thus able to stabilize a single-domain ferroelectric state coupled to a single antiferromagnetic spin cycloid (Figure 2b, right). Interestingly, using anisotropic strain in (111) films to design a single multiferroic state is a robust phenomenon as it can be applied to $BiFeO_3$ films grown on other scandates such as $TbScO_3(011)_o$ or $GdScO_3(011)_o$. While the strain state varies depending on the chosen scandate substrate (Figure S5), the anisotropy of the strain always imposes a single k_2 cycloid propagating along the a_o axis of the substrate (Figure S6).

Having stabilized this model $BiFeO_3$ system, we now investigate the influence of the film thickness on its multiferroic properties. RHEED oscillations attesting for the unit-cell by unit-cell growth of $BiFeO_3$ can be observed (**Figure 3a**) and bring unit-cell accuracy in our thickness determination. The two-dimensional growth is corroborated by the topography of the ultrathin films of $BiFeO_3$ (Figure 3b), which shows flat terraces and step heights of 0.23 nm, corresponding

to one unit cell along the [111] direction, i.e. $\boldsymbol{a} \times \sqrt{\mathbf{3}}/\mathbf{3}$ with $\boldsymbol{a}$ the pseudo-cubic unit-cell. Scanning NV magnetometry images acquired on $BiFeO_3$ films with thicknesses varying from 65 unit cells down to 3 unit cells are displayed in Figure 3c. For film thicknesses of 65 unit cells (15 nm), the $BiFeO_3$ film displays the aforementioned well-defined spin cycloid with a single propagation vector. Decreasing the film thickness down to 6 unit cells turns the magnetic configuration into a maze pattern. Further decreasing the film thickness to 4 and 3 unit cells, no magnetic stray field could be detected. Complementary measurements on $BiFeO_3$ wedged films (Figure S7) corroborate these findings with additional bubble-like domain structures at ultrathin limits before the collapse of the magnetic signal.

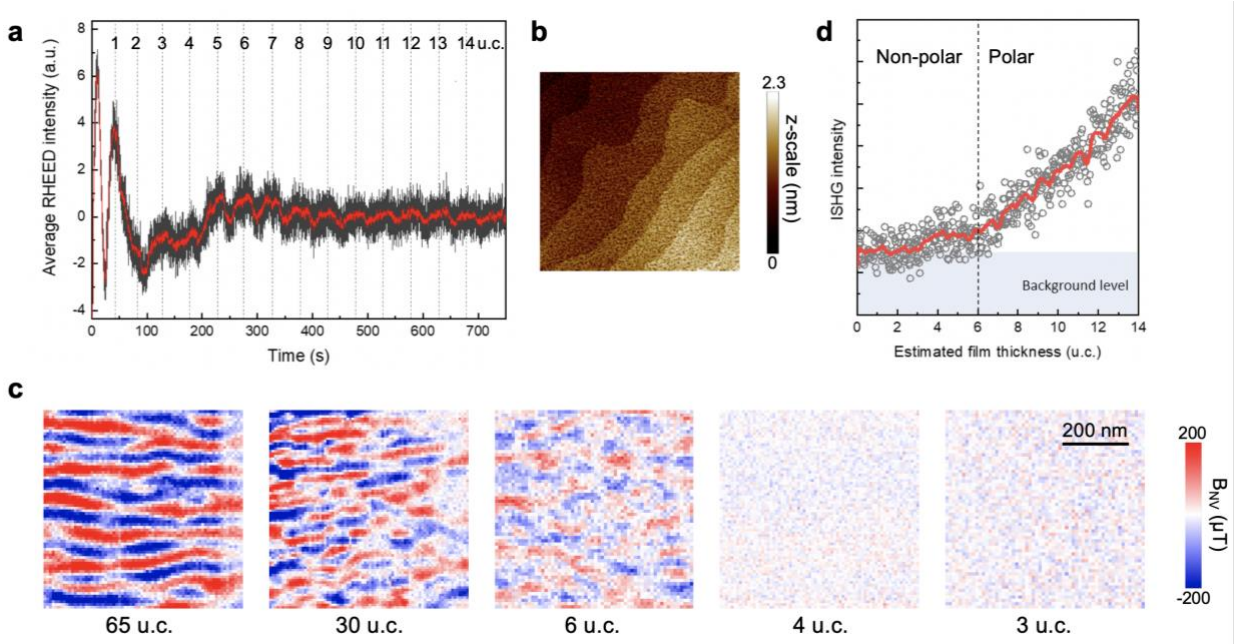

Figure 3. Onset of multiferroicity in ultrathin $BiFeO_3$. a) RHEED oscillations as function of the $BiFeO_3$ film thickness. The black line corresponds to the raw data while the red line is a result of adjacent averaging. b) Surface topography of a 6 unit-cell-thick $BiFeO_3$ thin film grown on $SrRuO_3$

(2 unit cells) buffered $DyScO_3(011)_o$. The size of the image is $2 \times 2\ \mu m^2$. c) Scanning NV magnetometry images of $BiFeO_3$ films with thicknesses of 65, 30, 6, 4, and 3 unit cells. d) In situ SHG monitoring of ferroelectricity as a function of the $BiFeO_3$ film thickness. The open circles correspond to raw data while the red line is a result of adjacent averaging.

In order to shed light on the suppression of the magnetic order in our films in the ultrathin regime, we monitored the onset of the ferroelectric order in the films with increasing thickness. Here, we used in situ optical second harmonic generation (ISHG)[28,29] to monitor the onset of ferroelectricity during the growth of the film (Figure 3d). To ensure layer-by-layer growth and to measure the film thickness in situ with unit-cell accuracy, we perform RHEED simultaneously with the ISHG measurement. While the ISHG signals remains at the background signal during the first unit cells, it starts increasing monotonously from the deposition of about 6 unit cells (1.4 nm), suggesting that ferroelectricity emerges at this thickness. This so-called critical thickness for the emergence of polarization in films is in good agreement with previously reported values for perovskite systems, yet in (001) orientation.[28,30] Most importantly, we highlight the perfect correspondence between the onset of a net polarization in our (111)-oriented films and that of the periodic magnetic stray field, signature of the spin cycloid. Hence, our results reveal unambiguously that the polarization-induced magnetoelectric interaction is at the origin of the non-collinear antiferromagnetic order.

Finally, we investigate the influence of the electric field on the polarization and antiferromagnetic state in our model system, single multiferroic domain $BiFeO_3$(111) thin films. Local piezoelectric loops acquired under the static PFM tip show a clear hysteresis of the vertical piezoresponse (Figure S2) that corresponds to a reversible 180° switching of the polarization from downward to upward with coercive voltages of +3 V and -1.5 V. This is corroborated by PFM imaging on a square area in which polarization was reversed by 180°, indicating the expected 180° phase shift of the VPFM as well as a similar amplitude as in the virgin state (Figure S8). In addition, using the trailing field of the scanning PFM tip[31] with a dc voltage, we could stabilize ferroelectric domains with in-plane variants. Indeed, in addition to the vertical polarization, three other ferroelastic variants, $\boldsymbol{P_2^{\pm}}$, $\boldsymbol{P_3^{\pm}}$ $\boldsymbol{P_4^{\pm}}$, are possible in the (111) films with a polarization respectively aligned along a, b, c of the pseudo-cubic unit cell (**Figure 4**b). We observe that the anisotropic strain on $BiFeO_3$(111) prevents the stabilization of some ferroelastic variants with the electric field. Indeed, only one $\boldsymbol{P_2^{\pm}}$ ferroelastic variant can be clearly written with the trailing field (Figure 4a, Note S2 for details), corresponding to the in-plane direction under tensile strain (Figure 4b). Scanning NV magnetometry was performed on an area containing $\boldsymbol{P_2^{+}}$ and $\boldsymbol{P_2^{-}}$ ferroelectric domains, as well as the initial $\boldsymbol{P_1^{-}}$ ferroelectric state (dashed square in Figure 4a). Despite the presence of three different ferroelectric variants, the image displayed in Figure 4d shows a periodic magnetic stray field corresponding to a cycloidal state propagating along a single k vector, parallel to the a_o of the substrate. Additional PFM and NV experiments on an area containing a $\boldsymbol{P_1^{+}}$ domain switched at 180° and a $\boldsymbol{P_2^{-}}$ domain switched at 71° (Figure S8) confirmed that manipulating ferroelectric domains in these $BiFeO_3$(111) films preserves the propagation vector of the antiferromagnetic cycloid. We are thus able to rotate the (P.k) cycloidal plane under

an electric field while preserving the uniaxial in-plane propagation direction, providing an interesting playground for the fundamental physics of the spin cycloid. Hence, we stabilized a model system to test the fundamental limits of the electric-field induced change in the cycloid propagation. Thickness dependencies and electric-field control of various polarization configurations may reveal new opportunities for electric-field control of the room temperature antiferromagnetic order at macroscopic scales.

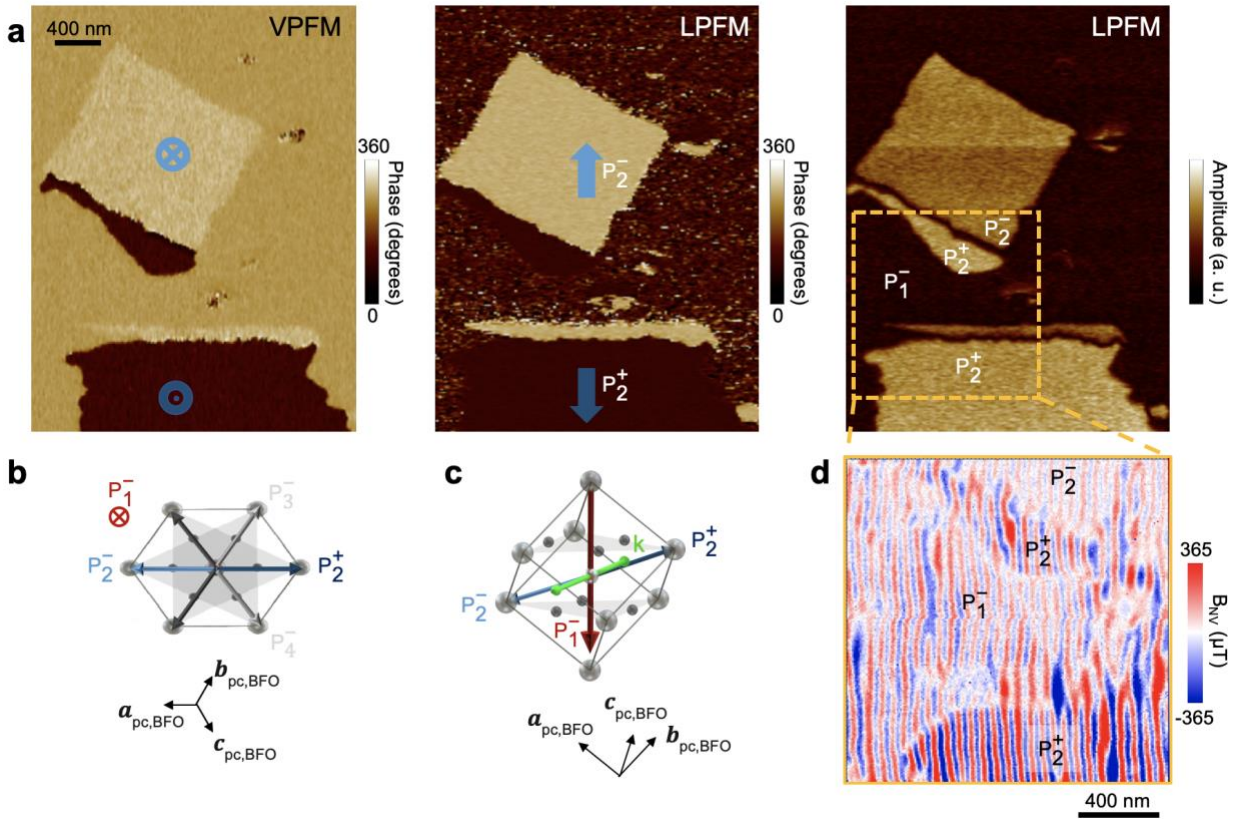

Figure 4. Electric-field manipulation of multiferroic domains. a) Vertical PFM phase (left), lateral PFM phase (middle) and amplitude (right) images in a zone containing domains defined with the trailing field of the PFM tip using a dc voltage of 2.5 V on a 50-nm-thick $BiFeO_3$ layer grown on a $SrRuO_3$-buffered $TbScO_3(011)_o$ substrate. Two types of ferroelectric domains, $\boldsymbol{P_2^+}$ and

$\boldsymbol{P_2^-}$, are stabilized corresponding to the same ferroelastic variant. b) Sketch of the $BiFeO_3$(111) surface under anisotropic strain with the surface projection of the three expected ferroelastic domains, $\boldsymbol{P_2^\pm}$, $\boldsymbol{P_3^\pm}$ $\boldsymbol{P_4^\pm}$, aligned along a_{pc}, b_{pc}, and c_{pc} of $BiFeO_3$, respectively. The distortion of the unit cell promotes only one ferroelastic variant aligned along the direction under tensile strain. c) Sketch of the pseudo-cubic unit cell of $BiFeO_3$ with the as-grown $\boldsymbol{P_1^-}$ ferroelectric state and the electrically-induced $\boldsymbol{P_2^+}$ and $\boldsymbol{P_2^-}$ states. The three polarization states share a common propagation vector, $\boldsymbol{k}$. d) Scanning NV magnetometry image of the area highlighted in (a), which contains $\boldsymbol{P_1^-}$, $\boldsymbol{P_2^+}$ and $\boldsymbol{P_2^-}$. The three ferroelectric domains share the same propagation vector, $\boldsymbol{k}$ of the cycloid, parallel to the in-plane a_o of the substrate.

In summary, single ferroelectric domain $BiFeO_3$(111) thin films were elaborated using pulsed laser deposition. Under isotropic in-plane strain on $SrTiO_3$(111), the films display multiple antiferromagnetic domains with spin cycloids propagating along the three equivalent in-plane directions. When resorting to anisotropic strain on $XScO_3(011)_o$ with X = Dy, Tb or Gd, the spin textures of the film turn to a single antiferromagnetic domain state with propagation vector along the a_o axis of the scandate substrate. Such a model $BiFeO_3$ thin film containing a single ferroelectric domain as well as a single spin cycloid opens perspectives for antiferromagnetic spintronics and magnonics. For instance, controlling antiferromagnetic domains should improve the propagation length of magnons in technologically-relevant thin films. Finally, we could detect the onset of the multiferroic state of such model system from ultrathin thickness limits of 1.4

nanometers. This reveals that as soon as the ferroelectric polarization emerges in $BiFeO_3$, the spin cycloid is stabilized by the magnetoelectric interaction.

Supporting Information. Methods, Figures S1-S9, Notes S1-S2.

Corresponding Author

*vincent.garcia@cnrs-thales.fr

Author Contributions

The manuscript was written through contributions of all authors. All authors have given approval to the final version of the manuscript. ‡These authors contributed equally.

Acknowledgements

We are grateful to Luis Moreno Vicente-Arche and Lucia Iglesias for their technical support with the pulsed laser deposition. We are thankful for support from the French Agence Nationale de la Recherche (ANR) through the project TATOO (ANR-21-CE09-0033), the European Union's Horizon 2020 research and innovation programme under the Grant Agreements No. 964931 (TSAR) and No. 866267 (EXAFONIS). This work is supported by a public grant overseen by the ANR as part of the "Investissements d'Avenir" program (Labex NanoSaclay, reference: ANR-10-LABX-0035). The Sesame Ile de France IMAGeSPIN project (No. EX039175) is also acknowledged. We also thank SOLEIL for providing beamtime under projects 20210810 and 99230027. M.T. and M. F. S. acknowledge the financial support by the Swiss National Science Foundation under project no. 200021_188414.

References

(1) Manipatruni, S.; Nikonov, D. E.; Young, I. A. Beyond CMOS Computing with Spin and Polarization. *Nature Phys* 2018, *14* (4), 338–343. https://doi.org/10.1038/s41567-018-0101-4.

(2) Manipatruni, S.; Nikonov, D. E.; Lin, C.-C.; Gosavi, T. A.; Liu, H.; Prasad, B.; Huang, Y.-L.; Bonturim, E.; Ramesh, R.; Young, I. A. Scalable Energy-Efficient Magnetoelectric Spin–Orbit Logic. *Nature* 2019, *565* (7737), 35–42. https://doi.org/10.1038/s41586-018-0770-2.

(3) Lebeugle, D.; Colson, D.; Forget, A.; Viret, M. Very Large Spontaneous Electric Polarization in BiFeO3 Single Crystals at Room Temperature and Its Evolution under Cycling Fields. *Appl. Phys. Lett.* 2007, *91* (2), 022907. https://doi.org/10.1063/1.2753390.

(4) Sosnowska, I.; Neumaier, T. P.; Steichele, E. Spiral Magnetic Ordering in Bismuth Ferrite. *J. Phys. C: Solid State Phys.* 1982, *15* (23), 4835–4846. https://doi.org/10.1088/0022-3719/15/23/020.

(5) Lebeugle, D.; Colson, D.; Forget, A.; Viret, M.; Bataille, A. M.; Gukasov, A. Electric-Field-Induced Spin Flop in BiFeO3 Single Crystals at Room Temperature. *Phys. Rev. Lett.* 2008, *100* (22), 227602. https://doi.org/10.1103/PhysRevLett.100.227602.

(6) Finco, A.; Haykal, A.; Fusil, S.; Kumar, P.; Dufour, P.; Forget, A.; Colson, D.; Chauleau, J.-Y.; Viret, M.; Jaouen, N.; Garcia, V.; Jacques, V. Imaging Topological Defects in a Noncollinear Antiferromagnet. *Phys. Rev. Lett.* 2022, *128* (18), 187201. https://doi.org/10.1103/PhysRevLett.128.187201.

(7) Chu, Y.-H.; Cruz, M. P.; Yang, C.-H.; Martin, L. W.; Yang, P.-L.; Zhang, J.-X.; Lee, K.; Yu, P.; Chen, L.-Q.; Ramesh, R. Domain Control in Multiferroic BiFeO3 through Substrate Vicinality. *Adv. Mater.* 2007, *19* (18), 2662–2666. https://doi.org/10.1002/adma.200602972.

(8) Chu, Y.-H.; He, Q.; Yang, C.-H.; Yu, P.; Martin, L. W.; Shafer, P.; Ramesh, R. Nanoscale Control of Domain Architectures in $BiFeO_3$ Thin Films. *Nano Lett.* 2009, *9* (4), 1726–1730. https://doi.org/10.1021/nl900723j.

(9) Giencke, J. E.; Folkman, C. M.; Baek, S.-H.; Eom, C.-B. Tailoring the Domain Structure of Epitaxial BiFeO3 Thin Films. *Current Opinion in Solid State and Materials Science* 2014, *18* (1), 39–45. https://doi.org/10.1016/j.cossms.2013.11.003.

(10) Ke, X.; Zhang, P. P.; Baek, S. H.; Zarestky, J.; Tian, W.; Eom, C. B. Magnetic Structure of Epitaxial Multiferroic BiFeO3 Films with Engineered Ferroelectric Domains. *Phys. Rev. B* 2010, *82* (13), 134448. https://doi.org/10.1103/PhysRevB.82.134448.

(11) Bertinshaw, J.; Maran, R.; Callori, S. J.; Ramesh, V.; Cheung, J.; Danilkin, S. A.; Lee, W. T.; Hu, S.; Seidel, J.; Valanoor, N.; Ulrich, C. Direct Evidence for the Spin Cycloid in Strained Nanoscale Bismuth Ferrite Thin Films. *Nat Commun* 2016, *7* (1), 12664. https://doi.org/10.1038/ncomms12664.

(12) Burns, S. R.; Sando, D.; Xu, B.; Dupé, B.; Russell, L.; Deng, G.; Clements, R.; Paull, O. H. C.; Seidel, J.; Bellaiche, L.; Valanoor, N.; Ulrich, C. Expansion of the Spin Cycloid in Multiferroic BiFeO3 Thin Films. *npj Quantum Mater.* 2019, *4* (1), 18. https://doi.org/10.1038/s41535-019-0155-2.

(13) Sando, D.; Appert, F.; Xu, B.; Paull, O.; Burns, S. R.; Carrétéro, C.; Dupé, B.; Garcia, V.; Gallais, Y.; Sacuto, A.; Cazayous, M.; Dkhil, B.; Le Breton, J. M.; Barthélémy, A.; Bibes, M.; Bellaiche, L.; Nagarajan, V.; Juraszek, J. A Magnetic Phase Diagram for Nanoscale Epitaxial $BiFeO_3$

Films. *Applied Physics Reviews* 2019, *6* (4), 041404. https://doi.org/10.1063/1.5113530.
(14) Kuo, C.-Y.; Hu, Z.; Yang, J. C.; Liao, S.-C.; Huang, Y. L.; Vasudevan, R. K.; Okatan, M. B.; Jesse, S.; Kalinin, S. V.; Li, L.; Liu, H. J.; Lai, C.-H.; Pi, T. W.; Agrestini, S.; Chen, K.; Ohresser, P.; Tanaka, A.; Tjeng, L. H.; Chu, Y. H. Single-Domain Multiferroic BiFeO3 Films. *Nat Commun* 2016, *7* (1), 12712. https://doi.org/10.1038/ncomms12712.
(15) Waterfield Price, N.; Johnson, R. D.; Saenrang, W.; Maccherozzi, F.; Dhesi, S. S.; Bombardi, A.; Chmiel, F. P.; Eom, C.-B.; Radaelli, P. G. Coherent Magnetoelastic Domains in Multiferroic BiFeO 3 Films. *Phys. Rev. Lett.* 2016, *117* (17), 177601. https://doi.org/10.1103/PhysRevLett.117.177601.
(16) Waterfield Price, N.; Johnson, R. D.; Saenrang, W.; Bombardi, A.; Chmiel, F. P.; Eom, C. B.; Radaelli, P. G. Electrical Switching of Magnetic Polarity in a Multiferroic BiFeO 3 Device at Room Temperature. *Phys. Rev. Applied* 2017, *8* (1), 014033. https://doi.org/10.1103/PhysRevApplied.8.014033.
(17) Waterfield Price, N.; Vibhakar, A. M.; Johnson, R. D.; Schad, J.; Saenrang, W.; Bombardi, A.; Chmiel, F. P.; Eom, C. B.; Radaelli, P. G. Strain Engineering a Multiferroic Monodomain in Thin-Film Bi Fe O 3. *Phys. Rev. Applied* 2019, *11* (2), 024035. https://doi.org/10.1103/PhysRevApplied.11.024035.
(18) Gross, I.; Akhtar, W.; Garcia, V.; Martínez, L. J.; Chouaieb, S.; Garcia, K.; Carrétéro, C.; Barthélémy, A.; Appel, P.; Maletinsky, P.; Kim, J.-V.; Chauleau, J. Y.; Jaouen, N.; Viret, M.; Bibes, M.; Fusil, S.; Jacques, V. Real-Space Imaging of Non-Collinear Antiferromagnetic Order with a Single-Spin Magnetometer. *Nature* 2017, *549* (7671), 252–256. https://doi.org/10.1038/nature23656.
(19) Haykal, A.; Fischer, J.; Akhtar, W.; Chauleau, J.-Y.; Sando, D.; Finco, A.; Godel, F.; Birkhölzer, Y. A.; Carrétéro, C.; Jaouen, N.; Bibes, M.; Viret, M.; Fusil, S.; Jacques, V.; Garcia, V. Antiferromagnetic Textures in BiFeO3 Controlled by Strain and Electric Field. *Nature Communications* 2020, *11* (1), 1704. https://doi.org/10.1038/s41467-020-15501-8.
(20) Zhong, H.; Finco, A.; Fischer, J.; Haykal, A.; Bouzehouane, K.; Carrétéro, C.; Godel, F.; Maletinsky, P.; Munsch, M.; Fusil, S.; Jacques, V.; Garcia, V. Quantitative Imaging of Exotic Antiferromagnetic Spin Cycloids in Bi Fe O 3 Thin Films. *Phys. Rev. Applied* 2022, *17* (4), 044051. https://doi.org/10.1103/PhysRevApplied.17.044051.
(21) Sando, D.; Agbelele, A.; Rahmedov, D.; Liu, J.; Rovillain, P.; Toulouse, C.; Infante, I. C.; Pyatakov, A. P.; Fusil, S.; Jacquet, E.; Carrétéro, C.; Deranlot, C.; Lisenkov, S.; Wang, D.; Le Breton, J.-M.; Cazayous, M.; Sacuto, A.; Juraszek, J.; Zvezdin, A. K.; Bellaiche, L.; Dkhil, B.; Barthélémy, A.; Bibes, M. Crafting the Magnonic and Spintronic Response of BiFeO3 Films by Epitaxial Strain. *Nature Mater* 2013, *12* (7), 641–646. https://doi.org/10.1038/nmat3629.
(22) Heron, J. T.; Trassin, M.; Ashraf, K.; Gajek, M.; He, Q.; Yang, S. Y.; Nikonov, D. E.; Chu, Y.-H.; Salahuddin, S.; Ramesh, R. Electric-Field-Induced Magnetization Reversal in a Ferromagnet-Multiferroic Heterostructure. *Phys. Rev. Lett.* 2011, *107* (21), 217202. https://doi.org/10.1103/PhysRevLett.107.217202.
(23) Heron, J. T.; Bosse, J. L.; He, Q.; Gao, Y.; Trassin, M.; Ye, L.; Clarkson, J. D.; Wang, C.; Liu, J.; Salahuddin, S.; Ralph, D. C.; Schlom, D. G.; Íñiguez, J.; Huey, B. D.; Ramesh, R. Deterministic Switching of Ferromagnetism at Room Temperature Using an Electric Field. *Nature* 2014, *516* (7531), 370–373. https://doi.org/10.1038/nature14004.
(24) Vaz, D. C.; Lin, C.-C.; Plombon, J.; Choi, W. Y.; Groen, I.; Arango, C.; Chuvilin, A.; Hueso, L.

E.; Nikonov, D. E.; Li, H.; Clendenning, S. B.; Gosavi, T. A.; Huang, Y.-L.; Prasad, B.; Ramesh, R.; Vecchiola, A.; Bibes, M.; Bouzehouane, K.; Fusil, S.; Garcia, V.; Young, I. A.; Casanova, F. Voltage-Based Magnetization Switching and Reading in Magnetoelectric Spin-Orbit Nanodevices. arXiv.org e-Print archive. 2023. https://doi.org/10.48550/arXiv.2302.12162. (accessed 2023-02-23)

(25) Basu, S. R.; Martin, L. W.; Chu, Y. H.; Gajek, M.; Ramesh, R.; Rai, R. C.; Xu, X.; Musfeldt, J. L. Photoconductivity in BiFeO3 Thin Films. *Appl. Phys. Lett.* 2008, *92* (9), 091905. https://doi.org/10.1063/1.2887908.

(26) Blok, J. L.; Wan, X.; Koster, G.; Blank, D. H. A.; Rijnders, G. Epitaxial Oxide Growth on Polar (111) Surfaces. *Appl. Phys. Lett.* 2011, *99* (15), 151917. https://doi.org/10.1063/1.3652701.

(27) Chauleau, J.-Y.; Chirac, T.; Fusil, S.; Garcia, V.; Akhtar, W.; Tranchida, J.; Thibaudeau, P.; Gross, I.; Blouzon, C.; Finco, A.; Bibes, M.; Dkhil, B.; Khalyavin, D. D.; Manuel, P.; Jacques, V.; Jaouen, N.; Viret, M. Electric and Antiferromagnetic Chiral Textures at Multiferroic Domain Walls. *Nature Materials* 2020, *19* (4), 386–390. https://doi.org/10.1038/s41563-019-0516-z.

(28) De Luca, G.; Strkalj, N.; Manz, S.; Bouillet, C.; Fiebig, M.; Trassin, M. Nanoscale Design of Polarization in Ultrathin Ferroelectric Heterostructures. *Nat Commun* 2017, *8* (1), 1419. https://doi.org/10.1038/s41467-017-01620-2.

(29) Sarott, M. F.; Gradauskaite, E.; Nordlander, J.; Strkalj, N.; Trassin, M. In Situ Monitoring of Epitaxial Ferroelectric Thin-Film Growth. *Journal of Physics: Condensed Matter* 2021, *33* (29), 293001. https://doi.org/10.1088/1361-648X/abf979.

(30) Junquera, J.; Ghosez, P. Critical Thickness for Ferroelectricity in Perovskite Ultrathin Films. *Nature* 2003, *422* (6931), 506–509. https://doi.org/10.1038/nature01501.

(31) Balke, N.; Choudhury, S.; Jesse, S.; Huijben, M.; Chu, Y. H.; Baddorf, A. P.; Chen, L. Q.; Ramesh, R.; Kalinin, S. V. Deterministic Control of Ferroelastic Switching in Multiferroic Materials. *Nature Nanotech* 2009, *4* (12), 868–875. https://doi.org/10.1038/nnano.2009.293.

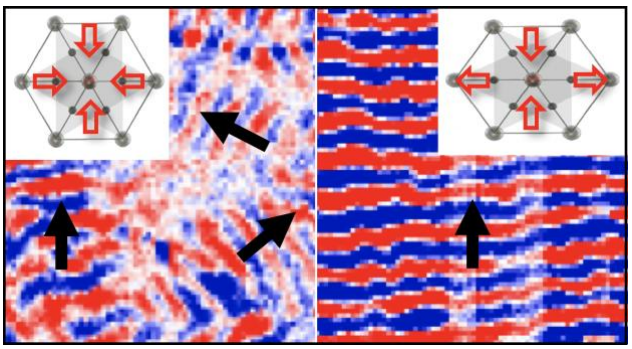

TOC Graphic